Solar-Sail Transfers from Invariant Objects to L5 Periodic Orbits

Fernandez Mora, Alvaro; Heiligers, Jeannette; Heaton, Andrew F.

Publication date
2018

Document Version
Accepted author manuscript

Published in
Proceedings of the 7th International Conference on Astrodynamics Tools and Techniques

SOLAR-SAIL TRANSFERS FROM INVARIANT OBJECTS TO L_5 PERIODIC ORBITS

Alvaro Fernandez, Andrew F. Heaton, and Jeannette Heiligers

Delft University of Technology, Delft, The Netherlands,
NASA Marshall Space Flight Center, Huntsville, Alabama,
and Delft University of Technology, Delft, The Netherlands

ABSTRACT

The continuing development of solar-sail technology in combination with the rising interest in a mission to the Sun-Earth L_5 point for heliophysics and the search for Trojan asteroids, raises the question of using solar sailing as the primary propulsion method to enable such a mission. This paper therefore investigates a range of solar-sail transfers to the L_5 point, departing from different invariant objects in the neighbourhood of Earth: natural and solar-sail displaced equilibrium points, families of periodic orbits and their associated stable invariant manifolds. Also, the arrival conditions are varied to be either natural or solar-sail displaced periodic orbits around the L_5 point. The transfers are obtained using a hybridisation of different trajectory design techniques. First, a multi-objective genetic algorithm is applied to obtain near-feasible initial guesses, which are transformed into feasible transfers using a differential correction method. Through a continuation on the fixed time of flight, the differential corrector is subsequently used to reduce the transfer time. As the differential corrector implements a stepwise constant control of the solar-sail attitude, a pseudospectral optimisation method is finally taken at hand to obtain a smooth, continuous control profile, to, if possible, further reduce the transfer time. This approach results in fast solar-sail transfers between 396 and 1194 days, depending on the departure and arrival configuration and the assumed solar-sail technology. These results can serve as preliminary design solutions for a mission to the Sun-Earth L_5 point.

Index Terms— Solar sailing, libration points, L_5 mission, genetic algorithm, differential correction, pseudospectral optimisation.

1. INTRODUCTION

The equilateral libration points of the Sun-Earth system are of interest for space missions related to space weather observations and the search for Trojan asteroids. Since these points are stationary 60 degrees ahead and behind Earth, they provide observational access to regions of the Sun that are inaccessible from Earth or the L_1 point. For example, the ACE satellite at the L_1 point allows the detection of geomagnetic storms approximately one hour before they arrive at Earth. A spacecraft at the equilateral points would enable a much earlier prediction of such space weather events. Furthermore, both equilateral points (L_4 and L_5) are suitable for studying coronal mass ejections (CMEs). However, only the L_5 point is useful for the study of corotating interaction regions as they pass by the L_5 point first and then Earth and the L_4 region. Additionally, a spacecraft at the L_4 or L_5 points enables a side view of events like solar flares and CMEs which would help in developing a better understanding of these events as well as the magnetic reconnection that triggers them [1].

Besides for space weather observation missions, the equilateral points are also of interest because of the potential presence of Trojan asteroids. Bodies in orbit around the L_4 and L_5 points are likely to have been there for a long time due to the stable character of orbits around the equilateral points. The study of such bodies can therefore help in understanding the formation of the Solar System. Trojan asteroids have been found in orbit around the equilateral points of the Sun-Mars, Sun-Earth, Sun-Jupiter, and Sun-Neptune systems as well as in systems such as Saturn with some of its moons [2]. In 2010, NASA's WISE spacecraft detected asteroid 2010TK$_7$ at the Sun-Earth L_4 point [2]. The fact that the STEREO spacecraft visited both equilateral points a year before, in 2009, without spotting asteroid 2010TK$_7$ suggests that there could still be other asteroids of small size or low albedo which have insofar not been discovered [2].

Due to the clear scientific relevance of the L_5 point, the literature holds a range of studies on transfers to the triangular points. For example, studies have shown the feasibility of transfers departing from 200 km altitude parking orbits around Earth to specific periodic orbits around the L_5 point. These transfers require a ΔV in the order of 4 km/s, depending on the targeted periodic orbit and desired time of flight [3, 4]. Solar sails are an excellent means to provide this high ΔV [5]. As an inexhaustible source of low thrust, it can significantly decrease, if not completely remove, the need for an onboard propellant. Moreover, Sood and Howell showed how, by using the invariant manifolds of Lyapunov orbits in combination with differential correction and optimisation, the use of a solar sail decreases the total ΔV for such a mission [6]. Alternatively, Farres, Heiligers and Miguel used Poincaré

sections and optimal control to compute solar-sail transfers between the Sun-Earth collinear points and the regions of practical stability around the equilateral libration points [7].

This paper builds on, and generalises, previous work on solar-sail transfers to the Sun-Earth L_5 point. In particular, a versatile approach is adopted to obtain solar-sail transfers departing from a range of invariant objects in the neighbourhood of Earth to entire families of L_5 periodic orbits. The invariant objects considered are equilibrium points, periodic orbits and their associated stable invariant manifolds. While previous work mostly focused on the planar, two-dimensional case and targeted specific initial and final conditions (e.g., a specific Earth parking orbit or a specific L_5 point orbit), this paper considers the three-dimensional case as well as entire families of periodic orbits for both the initial and final conditions.

2. DYNAMICAL SYSTEM

In order to model the motion of the solar-sail propelled spacecraft (hereafter in short referred to as "solar sail"), we consider the Circular Restricted Three-Body problem (CR3BP) perturbed with Solar Radiation Pressure (SRP). In such a model, the Sun and the Earth (primary bodies) move in circular orbits around their common barycenter exclusively attracting each other. The solar-sail (third body) motion is governed by the vector field induced by the gravitational pull of the primaries and the SRP. The primaries are assumed to be point masses and the solar sail is assumed to be massless.

The units of mass, distance and time are normalised such that the total mass of the system is 1, the Sun-Earth distance is 1 and the orbital period of the Earth around the Sun is 2π. With these normalised units, the gravitational parameter of Earth is $\mu = 3.0034806 \cdot 10^{-6}$ and the gravitational parameter of the Sun is $1-\mu$. We consider a synodic reference frame, $s(X, Y, Z)$, to study the system, where the X axis is defined along the Sun-Earth line pointing from the Sun to the Earth, the Z axis is defined in the direction of the angular momentum of the primaries and the Y axis completes the orthogonal reference frame.

In frame $s(X, Y, Z)$, the equations of motion can be obtained by including the inertial and non-inertial forces as:

$$\ddot{x} - 2\dot{y} = \frac{\partial \Omega}{\partial x} + a_x, \tag{1}$$

$$\ddot{y} + 2\dot{x} = \frac{\partial \Omega}{\partial y} + a_y, \tag{2}$$

$$\ddot{z} = \frac{\partial \Omega}{\partial z} + a_z, \tag{3}$$

with $\Omega = \frac{1}{2}\left(x^2+y^2\right) + \frac{1-\mu}{r_{sb}} + \frac{\mu}{r_{eb}}$, $r_{sb} = \sqrt{(x+\mu)^2+y^2+z^2}$ and $r_{eb} = \sqrt{(x+\mu-1)^2+y^2+z^2}$. The acceleration generated by the solar sail is defined as the vector $\boldsymbol{a} = [a_x \quad a_y \quad a_z]$ and it is produced by the transfer of momentum when solar photons are reflected by the sail. In this process, the properties of the sail and the solar flux determine how the force is produced. For the initial analyses in this paper, we assume a perfectly reflecting flat sail and a uniformly radiating Sun. More complex models account for the optical properties of the sail and geometry effects [5, 8, 9]. For an ideal sail, the SRP acceleration acts along the direction of the sail normal and is conveniently expressed as a function of the lightness number β. This parameter is defined as the ratio between the SRP and solar-gravitational accelerations [5]. Note that near-term values for this lightness number are $\beta \leq 0.04$ [10]. The SRP acceleration can then be described in dimensionless units as:

$$\boldsymbol{a} = \beta \frac{1-\mu}{r_{sb}^2} \langle \hat{\boldsymbol{r}}_{sb}, \boldsymbol{n} \rangle^2 \boldsymbol{n}, \tag{4}$$

where $\hat{\boldsymbol{r}}_{sb} = \frac{\boldsymbol{r_{sb}}}{r_{sb}}$, $\boldsymbol{r}_{sb} = [x+\mu \quad y \quad z]^T$ and $\boldsymbol{n}$ is the sail normal.

In order to describe the attitude of the sail, we follow [11] and define an orthonormal reference frame with its origin at the solar sail and basis $\{\hat{\boldsymbol{r}}_{sb}, \boldsymbol{p}, \boldsymbol{q}\}$, where $\boldsymbol{p} = \frac{\hat{\boldsymbol{r}}_{sb} \times \boldsymbol{k}}{|\hat{\boldsymbol{r}}_{sb} \times \boldsymbol{k}|}$ and $\boldsymbol{q} = \frac{\boldsymbol{p} \times \hat{\boldsymbol{r}}_{sb}}{|\boldsymbol{p} \times \boldsymbol{r}_{sb}|}$. The vector $\boldsymbol{k}$ denotes the unit vector along the Z axis. The sail normal can then be described in the orthonormal frame by two angles, known in the literature as the cone angle α and the clock angle δ, as $\boldsymbol{n} = \cos\alpha \boldsymbol{r} + \sin\alpha \sin\delta \boldsymbol{p} + \sin\alpha \cos\delta \boldsymbol{q}$. The equations of motion can then be expressed as:

$$\ddot{x} - 2\dot{y} = \frac{\partial \tilde{\Omega}}{\partial x} + a\left(-\frac{(x+\mu)z}{r_{sb}r_p}\sin\alpha\cos\delta + \frac{y}{r_p}\sin\alpha\sin\delta\right), \tag{5}$$

$$\ddot{y} + 2\dot{x} = \frac{\partial \tilde{\Omega}}{\partial y} + a\left(-\frac{yz}{r_{sb}r_p}\sin\alpha\cos\delta - \frac{x+\mu}{r_p}\sin\alpha\sin\delta\right), \tag{6}$$

$$\ddot{z} = \frac{\partial \tilde{\Omega}}{\partial z} + a\left(\frac{r_p}{r_{sb}}\sin\alpha\cos\delta\right), \tag{7}$$

where $a = \beta\frac{1-\mu}{r_{sb}^2}\cos^2\alpha$, $r_p = \sqrt{(x+\mu)^2+y^2}$ and $\tilde{\Omega} = \frac{1}{2}\left(x^2+y^2\right) + \left(1-\beta\cos^3\alpha\right)\frac{1-\mu}{r_{sb}} + \frac{\mu}{r_{eb}}$. The right-hand side of Eqs. 5-7 consist of two terms of different nature, where the terms included in $\tilde{\Omega}$ accept the form of a potential function. While the CR3BP is Hamiltonian, the SRP perturbation breaks this property of the system, but a few exceptions exist. For the cases where the non-potential terms in the equations of motion vanish, the system remains Hamiltonian. This happens when the sail normal is aligned with the direction of the Sun-sail line ($\alpha = 0$) and when the sail normal is perpendicular to the Sun-sail line ($\alpha = \pm\pi$). These cases are of particular interest because the existence of periodic and

quasi-periodic motion around equilibrium points is guaranteed. Another important aspect of the dynamical system when the Hamiltonian structure is preserved is the existence of a first integral $J_c = \dot{x}^2 + \dot{y}^2 + \dot{z}^2 - 2\tilde{\Omega}$, known as the Jacobi constant [11]. This constant of motion has important implications to characterise regions of possible motion and energy levels of periodic and quasi-periodic motion.

2.1. Invariant objects

Let us express Eqs. 5-7 as a system of first order differential equations given by:

$$\dot{\boldsymbol{x}} = f(\boldsymbol{x}, \alpha, \delta), \tag{8}$$

where $\boldsymbol{x} \in \mathbb{R}^6$ is a point in phase space. Let us also define the flow induced by f as $\phi_t(\boldsymbol{x}, \alpha, \delta)$ with $t \in \mathbb{R}$. A set $S \subset \mathbb{R}^6$ is invariant under the flow if for any element $\boldsymbol{u} \in S$, $\phi_t(\boldsymbol{u}, \alpha, \delta) \in S$ for any t [12]. When the angles α and δ are constant they act simply as parameters of the dynamics for which invariant sets can be defined. A wide variety of invariant sets exist in both the natural and SRP-CR3BP. Such sets can exist in the form of equilibrium points, periodic orbits, invariant manifolds or invariant tori. The first three will be discussed in more detail below, while invariant tori will be considered in future research.

2.1.1. Equilibrium points

It is well know that the CR3BP exhibits five equilibrium points known as the Lagrange points. It is also known that when SRP is included, different families of equilibrium points emerge [5, 11]. The surfaces of these so-called displaced equilibrium points are given by the following problem [5]:

$$-\nabla\Omega = \beta\frac{1-\mu}{r_{sb}^2}\langle\hat{\boldsymbol{r}}_{sb}, \boldsymbol{n}\rangle^2\boldsymbol{n} \tag{9}$$

$$\langle\hat{\boldsymbol{r}}_{sb}, \boldsymbol{n}\rangle \geq 0 \tag{10}$$

Note that, when the sail is oriented perpendicular to the Sun-sail line, the displaced equilibrium points reduce to the five natural Lagrange points. The displaced counterparts of the Lagrange points are referred to as SL_i with $i \in \{1, 2, .., 5\}$.

2.1.2. Periodic orbits

When the dynamical system is Hamiltonian, both periodic and quasi-periodic motion around the equilibrium points exist. In fact, these types of motion generally appear in continuous families. Numerous studies have used symmetric properties of the system to compute such families of periodic orbits in the natural system, e.g., [13, 14], and the SRP-perturbed system, e.g., [15, 16]. We, however do not exploit orbit symmetry to find periodic motion. A very general way to impose periodic motion is given by the definition of the map $G : \mathbb{R}^7 \to \mathbb{R}^6$ as [17]:

$$G(\boldsymbol{x}, T) = \phi_T(\boldsymbol{x}, \alpha, \delta) - \boldsymbol{x} \tag{11}$$

with $\boldsymbol{x} \in \mathbb{R}^6$ and $T \in \mathbb{R}_{>0}$. Note that the sail attitude is constant for each family of periodic orbits and therefore α and δ are fixed parameters of the map G. The search of periodic orbits is then transformed into finding $\{\boldsymbol{x}, T\}$ that solve $G(\boldsymbol{x}, T) = 0$. Such solutions can be found with a Newton method given a good initial guess. Let us assume $\hat{\boldsymbol{x}}$ and $\hat{T}$ are a guess for a solution. This guess can be corrected by linearising the periodicity equation and solving the linear system:

$$-G(\hat{\boldsymbol{x}}, \hat{T}) = JG(\hat{\boldsymbol{x}}, \hat{T})\begin{bmatrix}\delta\boldsymbol{x} \\ \delta T\end{bmatrix} \tag{12}$$

where JG denotes the Jacobian of G, and $\delta\boldsymbol{x}$ and δT denote the updates to the initial guess. The derivative of $\phi_T(\boldsymbol{x}, \alpha, \delta)$ with respect to the initial point can be obtained with the state transition matrix (STM) evaluated at time T denoted by $\Phi(\boldsymbol{x}, T, \alpha, \delta)$, yielding:

$$JG = \begin{bmatrix}\Phi(\boldsymbol{x}, T, \alpha, \delta) - I_{6\times6} & f(\phi_T(\boldsymbol{x}, \alpha, \delta), \alpha, \delta)\end{bmatrix}, \tag{13}$$

where $I_{6\times6}$ denotes the identity matrix. As can be seen, JG is of size 6×7 and is therefore not invertible. However, it is convenient to fix one of the components, x_i, of $\boldsymbol{x}$ to have control over what periodic orbit is computed. It is enough to set its variation δx_i to zero in Eq. 12, which is equivalent to eliminating δx_i from the updates vector and eliminating column i from JG, yielding the reduced Jacobian $\tilde{JG}$. The system can then be solved by inverting $\tilde{JG}$.

Given a solution $\{x^*, T^*\}$ for Eq. 11, continuation can be used to generate the whole family of periodic orbits. We choose to continue the family in the component x_i of $\boldsymbol{x}$. It is possible to obtain the unit tangent direction for a family of periodic orbits, $\boldsymbol{t}$, as the unit $Ker(JG(\boldsymbol{x}^*, T^*))$. The new guess is then obtained as [18]:

$$\begin{bmatrix}\hat{\boldsymbol{x}} \\ \hat{T}\end{bmatrix} = \begin{bmatrix}\boldsymbol{x}^* \\ T^*\end{bmatrix} + \delta S\boldsymbol{t} \tag{14}$$

where δS is the step size in the continuation.

In order to implement this method for the generation of families of periodic orbits, an initial guess is required. We obtained these guesses from the linearised flow at the equilibrium points.

An important feature of periodic orbits is their stability which can be assessed from the eigenvalues of the monodromy matrix $M = \Phi(\boldsymbol{x}, T, \alpha, \delta)$ for any point in a periodic orbit. Since we will only generate periodic orbits for the Hamiltonian case ($\alpha = 0$ or $\alpha = \pm\pi/2$), the monodromy matrix is symplectic. It can be shown that the characteristic polynomial of any symplectic matrix is reciprocal and consequently, the roots come in reciprocal pairs. Therefore, if λ is an eigenvalue, λ^{-1} is also an eigenvalue. It can also be shown

that for periodic orbits in autonomous Hamiltonian systems, one of the eigenvalues is equal to 1 with an associated eigenvector tangent to the orbit. Since the eigenvalues come in reciprocal pairs, the spectra of the monodromy matrix has the form [19]:

$$spec(M) = \{1, 1, \lambda_1, \lambda_1^{-1}, \lambda_2, \lambda_2^{-1}\}. \quad (15)$$

The stability indices are then defined as $s_i = |\lambda_i + \lambda_i^{-1}|$. With such definition, the behaviour around a periodic orbit can be described as:

- Hyperbolic: $s_i > 2$.
- Elliptic: $s_i < 2$. When $s_i = 2$ it is said to be parabolic.
- Complex unstable: if $\lambda_i \in \mathbb{C}\backslash\mathbb{R}$

A periodic orbit is said to be stable if $s_i \leq 2$ [20].

In this paper we consider only the planar Lyapunov, vertical Lyapunov and halo families, but several other exist [21]. As a first example, Fig. 1 shows the planar Lyapunov family around the SL_1 point for $\beta = 0.02$ and $\alpha = 0$ and the stability indices throughout the family. The values of the Jacobi constant for the smallest and biggest orbits have also been included for all families of periodic orbits presented. Since $s_1 > 2$ for the whole family, these orbits are unstable. However, the s_2 index shows that there is a set of more stable periodic orbits when $s_2 = 2$. For the vertical Lyapunov family depicted in Fig. 2, it can be seen that, again, $s_2 = 2$ for a set of orbits. The halo family and its stability indices shown in Fig. 3 show a range of orbits where both $s_1 = 2$ and $s_2 = 2$, therefore indicating that a few stable halo orbits exist. Lastly, the planar Lyapunov family around SL_5 and its stability indices depicted in Fig. 4 show that these orbits are stable, as both indices are parabolic.

2.1.3. Invariant manifolds

Let us assume $\boldsymbol{x}_0$ is a fixed (equilibrium) point of the non-linear system given by Eq. 8. The stable and center manifold theorems guarantee, under certain conditions, the existence of the stable manifold W^s, the unstable manifold W^u and the center manifold W^c; all of which are invariant under the flow. Such manifolds are tangent at $\boldsymbol{x}_0$ to the stable, unstable and center subspaces given by the stable, unstable and center directions of the linearisation of the non-linear system [12]. The stable and center manifold theorems also exist for periodic orbits. In that case, the invariant manifolds are tangent at the periodic orbit to the stable, unstable and center subspaces which are obtained from the linearisation of the flow around the cycle after one period, i.e., the monodromy matrix [12]. In this study, both the stable and unstable manifolds associated to fixed points or periodic orbits are used. Numerically, these invariant manifolds can be obtained by propagating the flow from an equilibrium point or a periodic orbit perturbed in the corresponding stable or unstable direction. The size of the perturbation selected is 10^{-5} in dimensionless units.

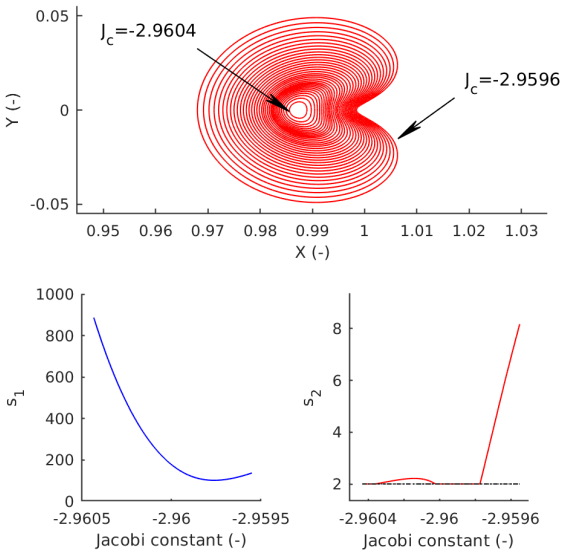

Fig. 1. Planar Lyapunov family around the SL_1 point for $\beta = 0.02$ and $\alpha = 0$ (top) and its stability indices (bottom).

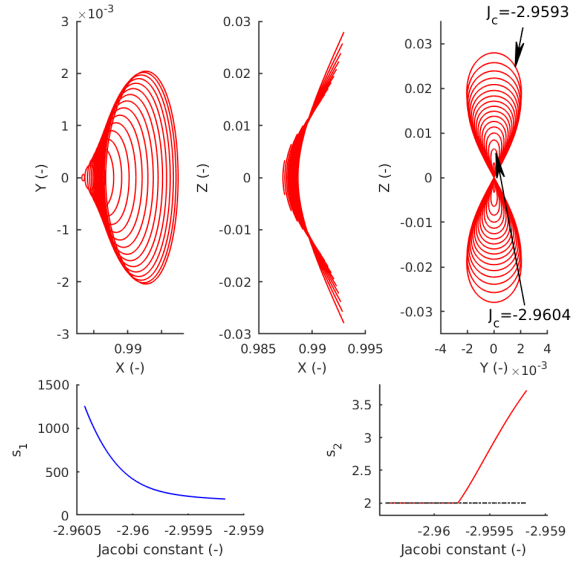

Fig. 2. Vertical Lyapunov family around the SL_1 point for $\beta = 0.02$ and $\alpha = 0$ (top) and its stability indices (bottom)

3. TRAJECTORY DESIGN

3.1. Genetic algorithm

A genetic algorithm (implemented using the Matlab® function *ga.m*) is taken at hand to solve a multi-objective optimisation problem in which a set of decision variables defines a guess for the transfer and the quality of that guess is as-

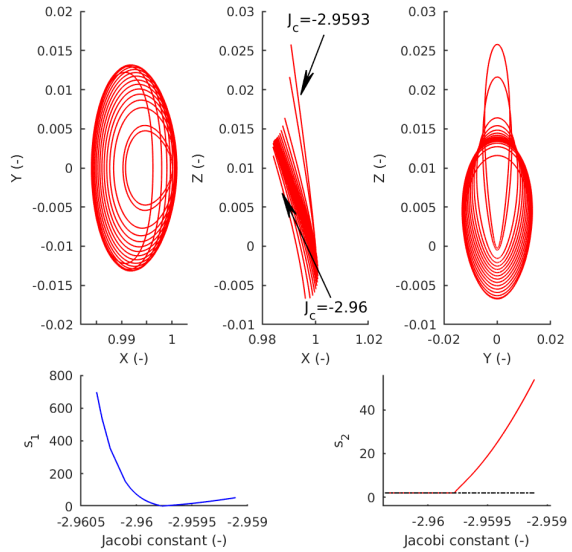

Fig. 3. Northern halo family around the SL_1 point for $\beta = 0.02$ and $\alpha = 0$ (top) and its stability indices (bottom)

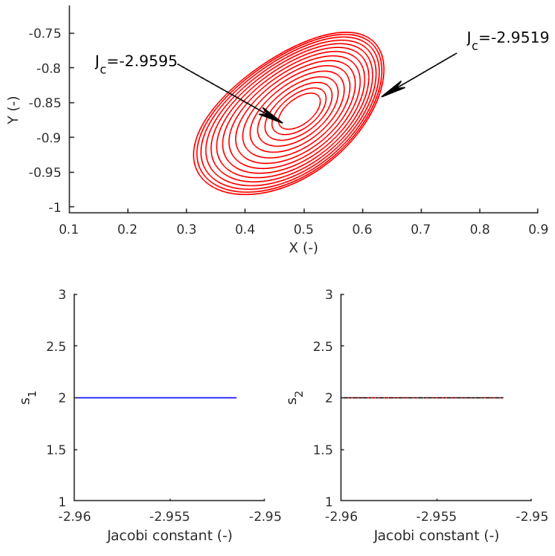

Fig. 4. Planar Lyapunov family around the SL_5 point for $\beta = 0.02$ and $\alpha = 0$ (top) and its stability indices (bottom)

sessed in terms of its infeasibility, ϵ_I, and the time of flight (TOF). Note that the decision variables vary depending on the case, i.e., the type of invariant object used as initial condition, which will each be discussed below.

3.1.1. Departure from collinear equilibrium points

If the initial condition is a natural collinear equilibrium point (L_1 or L_2) or a solar-sail displaced collinear equilibrium point (SL_1 or SL_2), the vector of decision variables, $\mathbf{x}$, is defined as:

$$\mathbf{x} = [d_f \quad \tau_f \quad \alpha_f] \tag{16}$$

Given a family of periodic orbits around the (displaced) L_5 point, the first variable, d_f, determines the dimensionless size of the periodic orbit as the largest distance from the periodic orbit to it associated equilibrium point. This variable allows to target transfers to entire families of orbits, as opposed to works that target one particular periodic orbit [4, 6]. The second variable, τ_f, determines the insertion point into the orbit which is obtained from propagating the flow over a time $\tau_f T$, where T is the periodic orbit period, starting from some reference point. Finally, a third variable, α_f, determines the constant cone angle of the sail which is used in the backwards integration from the insertion point over a five year period. Figure 5 depicts these variables and their effect on the trajectory.

The unstable manifolds originating from the (displaced) collinear equilibrium points are also integrated over a five year period, only forwards in time. However, note that these unstable manifolds enter a complex region around Earth for the natural Lagrange points [7] which can cause issues in the adopted approach. Therefore, for such cases, the trajectory starts from the equilibrium points perturbed in the direction of the unstable manifold but including a solar-sail acceleration where the solar sail is pitched at a fixed, zero degree angle with respect to the incoming solar radiation. It can be shown that with such an attitude and the solar-sail technology considered, the spacecraft diverts away from Earth.

The initial guess transfer is then given by the union of the unstable manifold of the (displaced) equilibrium point and the backwards flow from the periodic orbit at the point of minimum euclidean norm in dimensionless phase space. This value is used as the infeasibility objective, ϵ_I. Together with the corresponding time of flight, the genetic algorithm creates a Pareto front that gives a range of potential initial guesses that vary in feasibility and time of flight. Ideally, the initial guess selected for the next steps of the trajectory design process is the guess which is sufficiently feasible and has the smallest time of flight, where, by sufficiently feasible, it is meant that the differential correction can converge to a feasible solution from the initial guess.

As an example, Fig. 6 shows the pareto front obtained for transfers from the natural L_1 point to an SL_5 solar-sail planar Lyapunov orbit for $\beta = 0.02$. The initial guess highlighted in red is depicted in Fig. 7. In terms of objective values, this initial guess achieves a feasibility of $\epsilon_I = 0.0344$, which corresponds to an error in position of $2.15 \cdot 10^6$ km and an error in synodic velocity of 0.9292 km/s. The time of flight equals TOF $= 738$ days, while the values for the decision variables

are: $\mathbf{x} = [d_f \quad \tau_f \quad \alpha_f] = [0.1858 \quad 0.3227 \quad 28.89]$, where α_f is given in degrees.

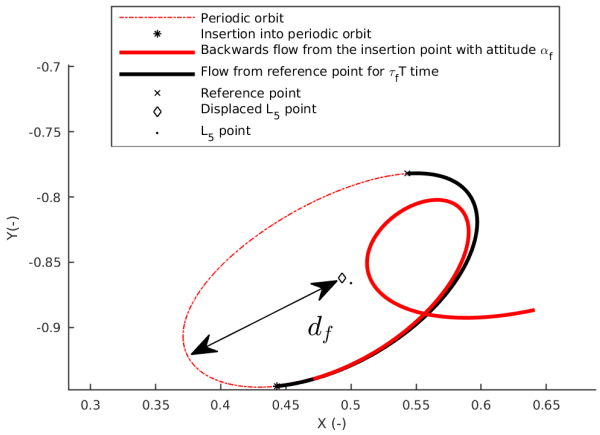

Fig. 5. Schematic of genetic algorithm decision vector variables.

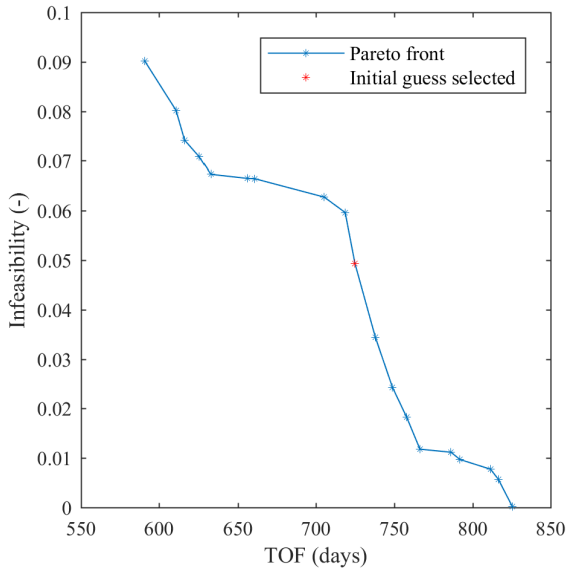

Fig. 6. Example of the Pareto front obtained with the genetic algorithm for transfers from the natural L_1 point to the family of SL_5 solar-sail planar Lyapunov orbits with $\beta = 0.02$.

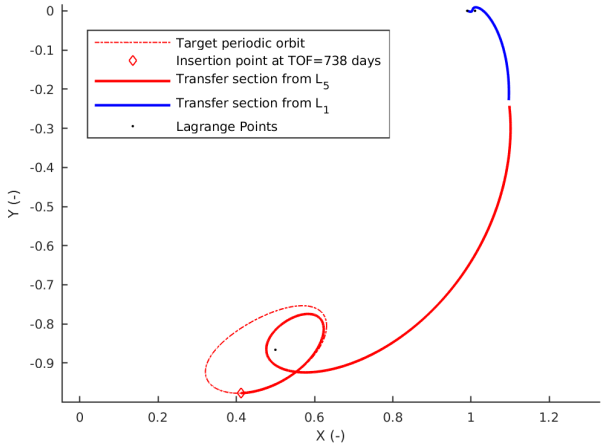

Fig. 7. Example of initial guess from the Pareto front for a transfer from the natural L_1 point to the family of SL_5 solar-sail planar Lyapunov orbits with $\beta = 0.02$.

3.1.2. Departure from periodic orbits around collinear libration points

When the departing invariant object is a periodic orbit within an orbit family around the L_1, L_2, SL_1 or SL_2 points, the decision vector in Eq. 16 is expanded to:

$$\mathbf{x} = [d_0 \quad \tau_0 \quad d_f \quad \tau_f \quad \alpha_f \quad \delta_f]. \tag{17}$$

Equation 17 now also includes decision variables to select the best size of the departing orbit, d_0, and the best departure condition along that orbit, τ_0. Furthermore, if the departing periodic orbit is a three-dimensional orbit, the angle δ_f considers a solar-sail attitude component in the out-of-plane direction in the backwards propagation from the L_5 region.

Since the periodic orbits around the collinear equilibrium points are unstable, they have associated unstable manifolds. The decision vector expressed in Eq. 17 defines a departure periodic orbit and the departing point. The departure conditions are propagated along the unstable manifold for a five year period—The initial guess is then again obtained as the union of the trajectory along the unstable manifold of the periodic orbit and the backwards flow from the periodic orbit around L_5 or SL_5at the point of minimum euclidean norm in dimensionless phase space.

The unstable manifolds of the natural periodic orbits around the collinear equilibrium points do not present the complex region around Earth that the manifolds associated to the natural collinear equilibrium points do. Nevertheless, the initial guesses benefit, in terms of TOF, from using the sail at a zero degree angle with respect to the incoming solar flux.

Therefore, the approach described for the unstable manifolds of the collinear Lagrange points is also adopted for the unstable manifolds of natural periodic orbits. When departing from solar-sail periodic orbits, their associated unstable manifolds already have a sail attitude aligned with the incoming flux. Therefore the true unstable manifolds are used.

3.1.3. Departure from stable manifold

The final case considered is the one where the solar-sail spacecraft is assumed to be launched as a secondary payload on a mission were the primary spacecraft is injected onto the the stable manifold of a particular halo orbit around the L_1 point where the stable manifold passes closest by Earth. It is further assumed that the solar sail is deployed at some point along that stable manifold. The vector of decision variables then is:

$$\mathbf{x} = [\tau_0 \quad \alpha_0 \quad \delta_0 \quad d_f \quad \tau_f \quad \alpha_f \quad \delta_f] \tag{18}$$

where τ_0 determines the departing conditions along the primary spacecraft trajectory; if T_p is the transfer time for the primary spacecraft along the stable manifold, the solar sail is deployed at $\tau_0 T_p$. The variables α_0 and δ_0 are the cone and clock angle for the segment departing from the stable manifold of the periodic orbit which is again propagated for five years. The remaining variables are analogous to the ones described in the previous cases. Note that δ_0 and δ_f are only used if the problem considered is not planar.

3.2. Multiple shooting differential corrector

The transfers obtained with the genetic algorithm are not yet feasible nor time-optimal. We use a multiple shooting differential corrector to first obtain feasible trajectories and then reduce the time of flight.

First, the guesses are discretised on $n = 30$ nodes. Each node contains a point in phase space, a cone angle, a clock angle and a temporal variable. They can be expressed as:

$$\boldsymbol{X}_i = \begin{bmatrix} \boldsymbol{x}_i \\ \alpha_i \\ \delta_i \\ t_i \end{bmatrix} \quad \text{for} \quad i \in \{1, 2, ...n\} \tag{19}$$

A feasible trajectory for a given TOF, T_0, with constraints g_0 and g_f on the initial and final nodes is obtained as the solution to the following problem:

$$g_0(\boldsymbol{X}_1) = 0 \tag{20}$$

$$\phi_{t_i}(\boldsymbol{x}_i, \alpha_i, \delta_i) - \boldsymbol{x}_{i+1} = 0 \quad \text{for} \quad i = \{1, 2, ...n-1\} \tag{21}$$

$$g_f(\boldsymbol{X}_n) = 0 \tag{22}$$

$$\sum_{i=1}^{n-1} t_i - T_0 = 0 \tag{23}$$

The constraints g_0 and g_f depend on the departure and arrival conditions selected. We can rewrite Eqs. 20-23 as $S(\boldsymbol{X}) = 0$, with $\boldsymbol{X} = [\boldsymbol{X}_1^T, \boldsymbol{X}_2^T, ...\boldsymbol{X}_n^T]^T$. Then, an initial guess $\hat{\boldsymbol{X}}$ can be updated by solving the linear system:

$$-S(\hat{\boldsymbol{X}}) = JS(\hat{\boldsymbol{X}})\delta\boldsymbol{X}, \tag{24}$$

where $JS(\boldsymbol{X})$ =

$$\begin{bmatrix} Jg_0(\boldsymbol{X}_1) & 0 & \cdots & \cdots & \cdots & \cdots & 0 \\ \tilde{\Phi}_1 & f_1 & -E & 0 & \cdots & \cdots & 0 \\ 0 & \tilde{\Phi}_2 & f_2 & -E & 0 & \cdots & 0 \\ \vdots & \ddots & \ddots & \ddots & \ddots & \ddots & \vdots \\ 0 & \cdots & \cdots & \tilde{\Phi}_{n-2} & f_{n-2} & -E & 0 \\ 0 & \cdots & \cdots & \cdots & \tilde{\Phi}_{n-1} & f_{n-1} & -E \\ 0 & \cdots & \cdots & \cdots & \cdots & \cdots & Jg_f(\boldsymbol{X_n}) \\ u & \cdots & \cdots & \cdots & \cdots & u & 0 \end{bmatrix}, \tag{25}$$

with $f_i = f(\phi_{t_i}(\boldsymbol{x}_i, \alpha_i, \delta_i), \alpha_i, \delta_i)$, $E = [I_{6\times6} \quad 0_{6\times3}]$, $u = [0_{1\times8} \quad 1]$ and $\tilde{\Phi}_i = \tilde{\Phi}(\boldsymbol{x}_i, t_i, \alpha_i, \delta_i)$. The 6×8 matrix $\tilde{\Phi}$ is an expanded STM that includes the variation of $\phi_{ti}(\boldsymbol{x}_i, \alpha_i, \delta_i)$ with respect to α_i and δ_i, i.e., $\tilde{\Phi} = [\Phi \quad \frac{\partial \phi_t}{\partial \alpha} \quad \frac{\partial \phi_t}{\partial \delta}]$ [6].

For some cases, the variables of the initial and final node, as they appear in Eq.19, need to be changed to define the constraints on them. Furthermore, the addition or elimination of variables for the outer nodes requires the Jacobian of $S(\boldsymbol{X})$, as it appears in Eq. 25, to be slightly modified to account for the variables used. Nevertheless, the general structure of $JS(\boldsymbol{X})$ is maintained.

3.2.1. Transfers considering fixed periodic orbits

Let us assume we want to fix node $\boldsymbol{X}_1$ or $\boldsymbol{X}_n$ to lie on a specific periodic orbit. Such periodic orbit can be described by a phase space point $\boldsymbol{x}_0$, a period T and cone and clock angles $\alpha = 0, \pi/2$ and $\delta = \pi/2$, respectively. Then the node $\boldsymbol{X}_i$ with $i = 1, n$ needs to satisfy:

$$\bar{G}(\boldsymbol{x}_i, t) = \phi_t(\boldsymbol{x}_0, \alpha, \delta) - \boldsymbol{x}_i = 0, \tag{26}$$

for some $t \in [0, T)$. If such constraint is implemented for the initial or final point, the node needs to include a variable for t in Eq. 26. Additionally, α_n and δ_n for the last node are not necessary as the attitude of the sail for the fixed periodic orbit is fixed. The initial and final nodes can then be expressed as:

$$\boldsymbol{X}_1 = \begin{bmatrix} \boldsymbol{x}_1 \\ \alpha_1 \\ \delta_1 \\ t_1 \\ t_1^* \end{bmatrix} \quad \boldsymbol{X}_n = \begin{bmatrix} \boldsymbol{x}_n \\ t_n^* \end{bmatrix}, \tag{27}$$

where t_1^* and t_n^* are used for the variable t in Eq. 26 for the fixed periodic orbit of the initial and final nodes respectively. Lastly, the Jacobian of $\bar{G}$ needed for the Newton method can be obtained as:

$$J\bar{G} = [-I_{6\times6} \quad f(\phi_t(\boldsymbol{x}_0, \alpha, \delta), \alpha, \delta)] \tag{28}$$

3.2.2. Transfers between a collinear equilibrium point and families of periodic orbits around the (displaced) L_5 point

This case is equivalent to fixing $\boldsymbol{x}_1$ to the desired departure collinear equilibrium point, $\boldsymbol{x}_{fixed}$, and imposing the constraint given by Eq. 11 to $\boldsymbol{X}_n$. The first node can then be expressed as in equation 19, whereas the last node only requires of a phase space point and the period of the orbit it belongs to. Therefore,

$$\boldsymbol{X}_1 = \begin{bmatrix} \boldsymbol{x}_1 \\ \alpha_1 \\ \delta_1 \\ t_1 \end{bmatrix} \quad \boldsymbol{X}_n = \begin{bmatrix} \boldsymbol{x}_n \\ T_n \end{bmatrix}. \tag{29}$$

The constraints on the outer nodes are then:

$$g_0(\boldsymbol{X}_1) = \boldsymbol{x}_1 - \boldsymbol{x}_{fixed}, \tag{30}$$

$$g_f(\boldsymbol{X}_n) = G(\boldsymbol{x}_n, T_n). \tag{31}$$

If $\boldsymbol{X}_n$ defines a periodic orbit from an specific family, the constraint given by Eq. 31 will generally set the last node to orbits belonging to that family. Since the families are continuous, the case where g_f sets the last node to a family of periodic orbits different from the one used for the initial guess is unlikely unless the periodic orbit of the initial guess is close enough to a bifurcation point.

3.2.3. Transfers between families of periodic orbits

If the initial point, $\boldsymbol{x}_1$, is constrained to be on a periodic orbit, the variables for the initial node, $\boldsymbol{X}_1$, as they appear in Eq. 19, are not sufficient to define the departing periodic orbit. It could be possible to expand $\boldsymbol{X}_1$ with an extra variable, T_1, which would be the period of the initial periodic orbit and impose Eq. 11 to the initial node in a similar way as was done for the last node with Eq. 31. However, this does not work well in practice because the departing periodic orbits considered are generally unstable and the proposed differential corrector would have difficulties converging to fast transfers. Therefore, in order to be able to let the initial node belong to a family of unstable periodic orbits around the collinear equilibrium points, a more robust periodicity constraint is implemented. Let us consider a set defined by a point $\boldsymbol{x}$, a parameter T and fixed cone and clock angles α and δ respectively. The complete set can be expressed as:

$$\Gamma = \{\boldsymbol{y} : \phi_t(\boldsymbol{x}, \alpha, \delta) - \boldsymbol{y} = 0 \quad \text{for} \quad t \in [0, T)\}. \tag{32}$$

Then, the set Γ defines a periodic orbit if for any $\boldsymbol{v} \in \Gamma$, $G(\boldsymbol{v}, T, \alpha, \delta) = 0$. This can be expressed as:

$$\tilde{G}(\boldsymbol{x}, T, t) = \phi_T(\phi_t(\boldsymbol{x}, \alpha, \delta)\alpha, \delta) - \phi_t(\boldsymbol{x}, \alpha, \delta) = 0, \tag{33}$$

with $t \in [0, T)$. Equation 33 is a more robust periodicity constraint as it allows to impose periodicity not at $\boldsymbol{x}$ but at $\phi_t(\boldsymbol{x}, \alpha, \delta)$. By the theorem of existence and uniqueness of differential equations [12], if $\phi_t(\boldsymbol{x}, \alpha, \delta)$ belongs to a periodic orbit, so will $\boldsymbol{x}$. This method can be successfully implemented in the differential corrector.

For this case, the initial and final nodes are expressed as:

$$\boldsymbol{X}_1 = \begin{bmatrix} \boldsymbol{x}_1 \\ \alpha_1 \\ \delta_1 \\ t_1 \\ T_1 \\ \tilde{t}_1 \end{bmatrix}, \quad \boldsymbol{X}_n = \begin{bmatrix} \boldsymbol{x}_n \\ T_n \\ \tilde{t}_n \end{bmatrix}, \tag{34}$$

where $\tilde{t}_1$ and $\tilde{t}_n$ are used for the variable t in $\tilde{G}$. The constraints on the initial and final node are then:

$$g_0(\boldsymbol{X}_1) = \tilde{G}(\boldsymbol{x}_1, T_1, \tilde{t}_1) = 0, \tag{35}$$

$$g_f(\boldsymbol{X}_n) = \tilde{G}(\boldsymbol{x}_n, T_n, \tilde{t}_n) = 0. \tag{36}$$

To include the new periodicity constraints, the Jacobian of $\tilde{G}$ is needed for the Newton method and it can be expressed as:

$$\begin{aligned} J\tilde{G} = [&(\Phi(T, \phi_t(\boldsymbol{x}, \alpha, \delta), \alpha, \delta) - I_{6\times 6})\Phi(t, \boldsymbol{x}, \alpha, \delta) \\ &f(\phi_T(\phi_t(\boldsymbol{x}, \alpha, \delta), \alpha, \delta)) \\ &(\Phi(T, \phi_t(\boldsymbol{x}, \alpha, \delta), \alpha, \delta) - I_{6\times 6}) f(\phi_t(\boldsymbol{x}, \alpha, \delta), \alpha, \delta)] \end{aligned} \tag{37}$$

Note, that in section 3.2.2, the constraint G could be used to set the final node on a family of periodic orbits. This is possible only because such orbits are stable. The constraint $\tilde{G}$ can also be used in such transfers, but the results obtained are almost identical.

3.2.4. Transfers between the stable manifold of an orbit around a collinear equilibrium point and families of periodic orbits around the (displaced) L_5 point

This case corresponds to the scenario where the solar sail is launched as a secondary payload and the primary spacecraft is injected into the stable manifold of an orbit around a collinear equilibrium points. The multiple shooting differential corrector is described for the general case, but here only the case where the primary spacecraft targets a halo orbit around the L_1 point is considered.

The constraint $\bar{G}$ in Eq. 26 can be used as the constraint on the initial node. However, the point $\boldsymbol{x}_0$ that defined the fixed periodic orbit now corresponds to the closest point to Earth of the selected periodic orbit stable manifold. The angles α and δ are the cone and clock angles for the selected periodic orbit of the primary mission.

The node $\boldsymbol{X}_1$ needs to include the variable $t^\star$ for the dimensionless time spent on the stable manifold. For the constraint on the final node, g_f, both G (Eq. 11) and $\tilde{G}$ (Eq. 33) can be used. However, we choose the stronger periodicity constraint $\tilde{G}$. Therefore, the initial and final node can be

expressed as:

$$\boldsymbol{X}_1 = \begin{bmatrix} \boldsymbol{x}_1 \\ \alpha_1 \\ \delta_1 \\ t_1 \\ t^\star \end{bmatrix}, \quad \boldsymbol{X}_n = \begin{bmatrix} \boldsymbol{x}_n \\ T_n \\ \tilde{t}_n \end{bmatrix} \tag{38}$$

and the constraints on them are

$$g_0(\boldsymbol{X}_1) = \bar{G}(\boldsymbol{x}_1, t^\star) = 0, \tag{39}$$

$$g_f(\boldsymbol{X}_n) = \tilde{G}(\boldsymbol{x}_n, T_n, \tilde{t}_n) = 0. \tag{40}$$

3.2.5. Optimisation with the multiple shooting differential corrector

So far, the differential corrector described will compute transfers for a fixed TOF. In order to optimise the transfers with respect to the TOF, first the initial guess given by the genetic algorithm is converged with the differential corrector to a feasible trajectory with the TOF, T_0, of the initial guess. This solution is then used to compute a new solution for a TOF$= \kappa T_0$, with $\kappa < 1$. This process is iterated until the differential corrector cannot converge. Then, the factor κ is increased to allow smaller steps in the continuation. We use $\kappa \in [0.95 \quad 0.98 \quad 0.99 \quad 0.999 \quad 0.9995 \quad 0.9999 \quad 0.99999]$.

3.3. Optimal control solver PSOPT

The transfers obtained with the differential corrector are not necessarily optimal in the sense that the optimality conditions of the problem under consideration have not been checked or used to compute the solution. Therefore, we use the optimal control solver PSOPT, which is a C++ implementation of the direct Legendre pseudospectral method [22]. We set the objective as the TOF and include event constraints on the initial and final nodes. When the departing point is a collinear equilibrium point, the event constraint is defined by simply setting the initial node equal to the desired departing collinear equilibrium point. When the initial or final node are constrained to belong to a periodic orbit, we take the orbit given by the differential corrector, express it in a Fourier series and set the node to satisfy such series for some value of the angle that parameterises it. This angle is optimised as an static parameter in PSOPT.

4. RESULTS

We first apply the methodology described for transfers between the collinear equilibrium points and natural and solar sail families of planar Lyapunov periodic orbits (PLOs) around the L_5 and SL_5 points. This results in the time of flights for the differential correction + continuation (DC) and PSOPT approaches as in Table 1 for a range of lightness numbers.

When comparing the results obtained with the differential corrector and with PSOPT, PSOPT sometimes converges to slightly different transfer times for transfers starting from the natural or displaced L_1 points. This is mainly due to the fact that the initial guesses for these cases include close Earth approaches or multi-revolution spirals around Earth, which introduces convergence difficulties for both methods. The differences are most noticeable for lightness numbers of 0.01 and 0.05. On the other hand, when the transfers depart from the natural or displaced L_2 points, both PSOPT and the differential corrector converge to practically the same solution.

Generally, the optimised transfers with PSOPT are very close to the ones obtained with the differential corrector + continuation, indicating that PSOPT is not capable of further reducing the TOF beyond that obtained with the differential correction + continuation. It is therefore concluded that the differential corrector in combination with the continuation method is an efficient tool to optimise the transfers considered. Therefore, from this point on, only the differential corrector will be used to optimise the trajectories.

Table 2 shows the results obtained for transfers between families of planar Lyapunov orbits around the collinear equilibrium points and the (displaced) L_5 point. The results show that it is always faster to travel between families of natural periodic orbits. When comparing the TOF for transfers departing from the collinear equilibrium points and transfers departing from families of periodic orbits it can be seen that, for some cases, the differential corrector converges to faster solutions when departing from an equilibrium point than when departing from a planar Lyapunov periodic orbit around it. Generally, both cases have very similar TOFs with the exception of the cases with $\beta = 0.01$. In these cases, departing from periodic orbits can reduce the TOF by over 100 days. Figure 8 shows the TOF as a function of the lightness number for transfers departing from both the collinear equilibrium points (top) and from planar Lyapunov orbits around them (bottom), where the suffix "n" or "s" denotes natural and solar-sail orbits respectively, and the prefix "L" denotes departure from Lyapunov orbits. It is then clear that the larger the lightness number, the smaller the TOF. It can also be seen that the improvement in TOF with respect to an improvement in the sail performance decreases with increasing lightness number.

To visualise the transfers, Fig. 9 shows transfers for three cases: departing from L_1, departing from a natural planar Lyapunov orbit around L_1 and departing from a natural halo orbit around L_1. In all three cases, the target orbits belong to the natural planar family around L_5 and the sail performance is assumed to be $\beta = 0.02$. The transfer from the family of halo orbits has been included to demonstrate the capability of the differential corrector for non-planar cases. Figure 10 shows a three-dimensional close-up of the transfers in the neighbourhood of Earth. The TOF for the three cases is relatively similar.

The last case considered is when the solar sail is deployed

Table 1. TOF in days for transfers from the collinear equilibrium points to families of planar Lyapunov periodic orbits around the L_5 and SL_5 points

	$\beta = 0.01$		$\beta = 0.02$		$\beta = 0.03$		$\beta = 0.04$		$\beta = 0.05$	
Method	DC	PSOPT	DC	PSOPT	DC	PSOPT	DC	PSOPT	DC	PSOPT
$L_1 \rightarrow$ natural PLOs	943	962	612	613	486	486	434	435	402	418
$L_1 \rightarrow$ solar-sail PLOs	1094	1061	729	727	575	574	512	513	478	524
$SL_1 \rightarrow$ natural PLOs	1094	1019	685	686	563	570	512	525	481	496
$SL_1 \rightarrow$ solar-sail PLOs	1194	1136	801	803	651	664	589	605	555	611
$L_2 \rightarrow$ natural PLOs	846	846	599	598	481	480	429	428	396	396
$L_2 \rightarrow$ solar-sail PLOs	941	940	712	711	571	570	508	508	474	477
$SL_2 \rightarrow$ natural PLOs	920	919	672	671	551	550	494	493	458	457
$SL_2 \rightarrow$ solar-sail PLOs	1015	1014	784	783	642	647	575	574	509	494

Table 2. TOF in days for transfers from families of planar Lyapunov orbits around the collinear equilibrium points to families of planar Lyapunov orbits around the L_5 and SL_5 points

	$\beta = 0.01$	$\beta = 0.02$	$\beta = 0.03$	$\beta = 0.04$	$\beta = 0.05$
Natural PLOs around $L_1 \rightarrow$ natural PLOs	862	622	483	433	404
Natural PLOs around $L_1 \rightarrow$ solar-sail PLOs	978	728	580	513	476
Solar-sail PLOs around $SL_1 \rightarrow$ natural PLOs	947	668	545	500	455
Solar-sail PLOs around $SL_1 \rightarrow$ solar-sail PLOs	1041	804	641	576	525
Natural PLOs around $L_2 \rightarrow$ natural PLOs	812	579	454	427	405
Natural PLOs around $L_2 \rightarrow$ solar-sail PLOs	902	686	559	490	460
Solar-sail PLOs around $SL_2 \rightarrow$ natural PLOs	908	684	546	500	456
Solar-sail PLOs around $SL_2 \rightarrow$ solar-sail PLOs	920	672	551	494	458

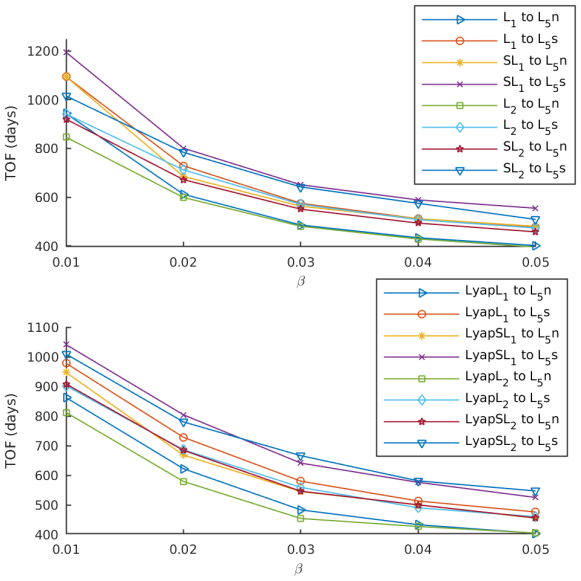

Fig. 8. Time of flight as a function of the lightness number for transfers departing from the collinear equilibrium points (top) and from planar Lyapunov orbits (bottom).

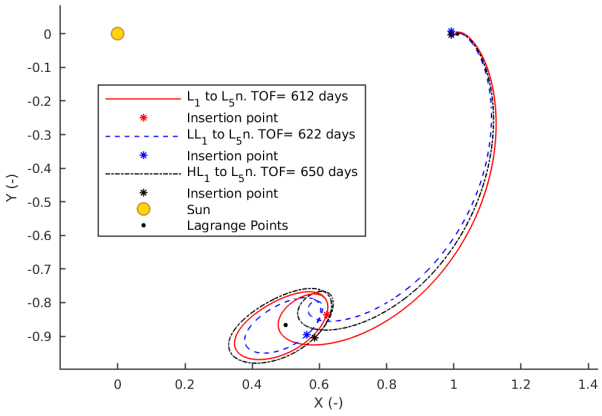

Fig. 9. Transfers to natural periodic orbits around L_5 departing from L_1 and departing from a natural planar Lyapunov and a natural halo orbit around L_1.

along the stable manifold, i.e., along the trajectory of the primary spacecraft towards a natural halo orbit. Such transfer is assumed to be along the stable manifold of the target halo orbit. The assumed halo orbit is characterised by a maximum dimensionless displacement of 0.01 dimensionless length units from L_1, which is equivalent to 1.49 million km. The departing point for the primary mission is at 0.47 million km from Earth and with an initial velocity of 1.15 km/s. It is also assumed that the sail performance is $\beta = 0.02$. The TOF for the primary mission is 237 days. Figure 11 shows the trans-

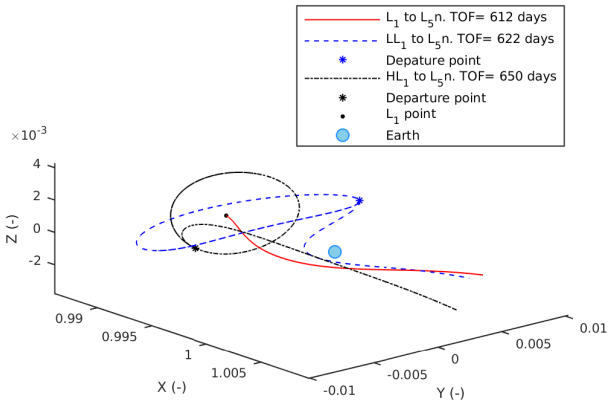

Fig. 10. Close-up of the transfers from Figure 9 in the neighbourhood of Earth

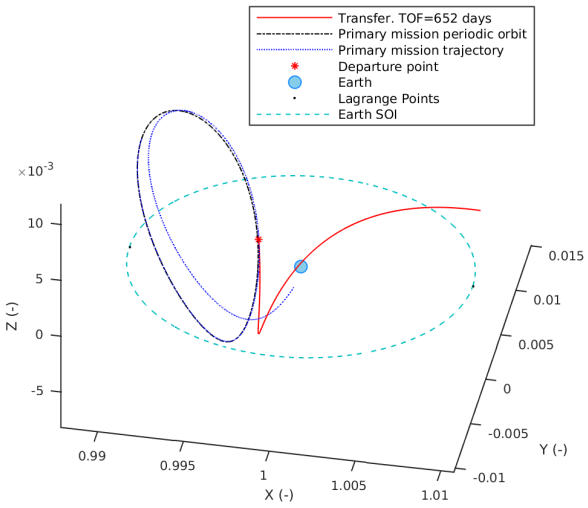

Fig. 12. Close-up in the neighbourhood of Earth for the transfer shown in Fig. 11

fer obtained with the differential corrector and Fig. 12 shows a close-up in the neighbourhood of Earth. The black arrows show the sail normal throughout the transfer. The TOF for the solar sail is 138 days for the first segment where the primary spacecraft goes from the neighbourhood of Earth to the point of separation of the solar sail spacecraft and 652 days for the second segment where the solar sail actively transfers to the L_5 region.

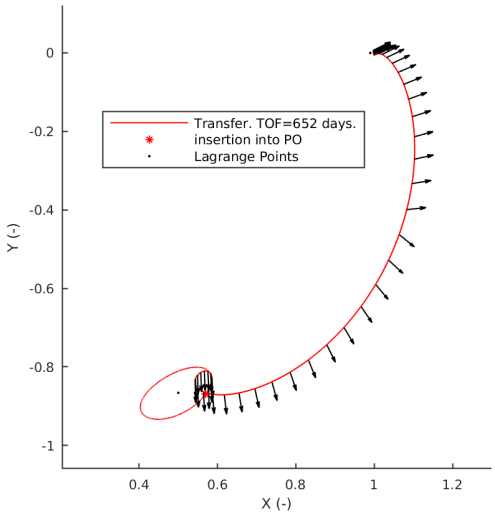

Fig. 11. Transfer for the secondary payload case with $\beta = 0.02$

5. CONCLUSIONS

We investigated solar-sail transfers between invariant objects in the neighbourhood of Earth and families of periodic orbits around the (displaced) L_5 point. The novel methodology introduced allows to consider fixed points, fixed periodic orbits, full families of periodic orbits and the stable manifold of orbits, showing the versatility of the differential corrector approach. Initial guesses were computed with the use of a genetic algorithm. Such guesses converge to feasible trajectories with a versatile multiple shooting differential corrector which allows to consider whole families of periodic orbits as departure and arrival conditions of the transfers. The differential corrector then selects the best orbits to depart from and to target. The multiple shooting differential corrector in combination with a continuation method furthermore allows to reduce the TOF of the transfers. Lastly, the optimal control solver PSOPT was used to attempt to further optimise the trajectories.

The results show that the genetic algorithm successfully obtains sufficiently feasible transfers that can then converge to feasible trajectories with the differential corrector. The optimal control solver PSOPT generally obtains very similar transfers to the ones obtained with the differential corrector + continuation, proving the latter to be a powerful tool for the problem under consideration. However, the control profile used in the differential corrector is of constant step-wise cone and clock angles, whereas PSOPT can offer a more continuous profile.

Fast solar-sail transfers taking between 396 and 1194

days, depending on the sail performance and the case, were computed. For the range of lightness numbers, β, explored, the TOF decreases with increasing β. It was also seen that the improvement in TOF with respect to the sail performance decreases with increasing β. Furthermore, for most cases, departing from periodic orbits is faster than when departing from equilibrium points. This is specially true when $\beta = 0.01$. Finally, it is always faster to travel between natural invariant objects than to travel between solar-sail invariant objects.

6. REFERENCES

[1] Gopalswamy, N., Davila, J. M., Cyr, O. C. St., Sittler, E. C., Auchère, F., Duvall, Jr. T. L., Hoeksema, J. T., Maksimovic, M., MacDowall, R. J., Szabo, A. and Collier, M. R., "Earth-Affecting Solar Causes Observatory (EASCO): A potential International Living with a Star Mission from Sun-Earth L_5," *Journal of Atmospheric and Solar-Terrestrial Physics*, vol. 73, no. 5-6, pp. 658–663, 2011.

[2] John, K. K. and Graham, L. D. and Abell, P. A., "Investigating Trojan Asteroids at the L_4/L_5 Sun-Earth Lagrange Points," 2015.

[3] Llanos, P. J., Miller, J. K. and Hintz, G. R., "L_5 Mission Design Targeting Strategy," in *AAS/AIAA Astrodynamicist Specialist Conference, Kauai, Hawaii, USA*, 2013.

[4] Lo, M. W., Llanos, P. J. and Hintz, G. R., "An L_5 Mission to Observe the Sun and Space Weather, Part I," in *AAS/AIAA Astrodynamicist Specialist Conference, San Diego, California, USA*, 2010.

[5] McInnes, C. R., *Solar Sailing - Technology, Dynamics and Mission Applications*, Springer, 2017.

[6] Sood, R. and Howell, K., "L_4, L_5 Solar Sail Transfers and Trajectory Design: Solar Observations and Potential Earth Trojan Exploration," in *26th AAS/AIAA Space Flight Mechanics Meeting, Napa, California, USA*, 2016.

[7] Farrés, A., Heiligers, J. and Miguel, N., "Road Map to L_4/L_5 with a solar sail," in *AIAA 2018-0211 Space Flight Mechanics Meeting, Kissimmee, Florida, USA*, 2018.

[8] Rios-Reyes, L. and Scheeres, D. J., "Generalized Model for Solar Sails," *Journal of Spacecraft and Rockets*, vol. 42, no. 1, pp. 182–185, 2005.

[9] Campbell, B. A. and Thomas, S. J., "Realistic Solar Sail Thrust," in *Advances in Solar Sailing*, pp. 407–435. Springer, 2014.

[10] Heiligers, J., J. M. Fernandez, O. R. Stohlman and W. K. Wilkie (2018), "Trajectory Design for a Solar-Sail Mission to Asteroid 2016 HO3," in *AAS/AIAA Astrodynamics Specialist Conference. Snowbird, Utah, USA*.

[11] Farrés, A., "Transfer Orbits to L_4 with a Solar Sail in the Earth-Sun System," *Acta Astronautica*, vol. 137, pp. 78–90, 2017.

[12] Perko, L., *Differential Equations and Dynamical Systems*, vol. 7, Springer Science & Business Media, 2013.

[13] Breakwell, J. V. and Brown, J. V., "The Halo Family of 3-Dimensional Periodic Orbits in the Earth-Moon Restricted 3-Body Problem," *Celestial Mechanics*, vol. 20, no. 4, pp. 389–404, 1979.

[14] Howell, K. C., "Three-Dimensional, Periodic, Halo orbits," *Celestial Mechanics*, vol. 32, no. 1, pp. 53–71, 1984.

[15] Waters, T. J. and McInnes, C. R., "Periodic Orbits Above the Ecliptic in the Solar-Sail Restricted Three-Body Problem," *Journal of Guidance, Control, and Dynamics*, vol. 30, no. 3, pp. 687–693, 2007.

[16] Heiligers, J. and Macdonald, M. and Parker, J. S., "Extension of Earth-Moon Libration Point Orbits with Solar Sail Propulsion," *Astrophysics and Space Science*, vol. 361, no. 7, pp. 241, 2016.

[17] Szebehely, V., *Theory of Orbit: The Restricted Problem of three Bodies*, Elsevier, 2012.

[18] Keller, H. B., "Lectures on Numerical Methods in Bifurcation Problems," *Applied Mathematics*, 1987.

[19] Arnold, V. I. and Kozlov, V. V. and Neishtadt, A. I., *Mathematical Aspects of Classical and Celestial Mechanics*, vol. 3, Springer Science & Business Media, 2007.

[20] Farrés, A., "Contribution to the Dynamics of a Solar Sail in the Earth-Sun System," *Doctorial thesis, Universitat de Barcelona*, 2009.

[21] E. J. Doedel, A. V. Romanov, R. C. Paffenroth, H. B. Keller, D. J. Dichmann, J. Galn-Vioque, and A. Vanderbauwhede, "Elemental Periodic Orbits Associated with the Libration Points in the Circular Restricted 3-Body Problem," *International Journal of Bifurcation and Chaos*, vol. 17, no. 08, pp. 2625–2677, 2007.

[22] Becerra, V. M., "Solving complex optimal control problems at no cost with PSOPT," in *Computer-Aided Control System Design (CACSD), 2010 IEEE International Symposium on*. IEEE, 2010, pp. 1391–1396.